In Situ Mechanical Characterization of the Cell Nucleus by Atomic Force Microscopy

Haijiao Liu,[†,‡,∥] Jun Wen,[†,∥] Yun Xiao,[‡] Jun Liu,[†] Sevan Hopyan,[§,⊥] Milica Radisic,[‡] Craig A. Simmons,[†,‡,*] and Yu Sun[†,‡,*]

[†]Department of Mechanical and Industrial Engineering, University of Toronto, Toronto, Ontario, Canada M5S 3G8, [‡]Institute of Biomaterials and Biomedical Engineering, University of Toronto, Toronto, Ontario, Canada M5S 3G9, [§]Development and Stem Cell Biology Program and Division of Orthopaedics, The Hospital for Sick Children, Toronto, Ontario, Canada M5G 1X8, and [⊥]Department of Molecular Genetics, University of Toronto, Toronto, Ontario, Canada M5S 1A8. [∥]These authors contributed equally to this work.

ABSTRACT The study of nuclear mechanical properties can provide insights into nuclear dynamics and its role in cellular mechanotransduction. While several methods have been developed to characterize nuclear mechanical properties, direct intracellular probing of the nucleus *in situ* is challenging. Here, a modified AFM (atomic force microscopy) needle penetration technique is demonstrated to mechanically characterize cell nuclei *in situ*. Cytoplasmic and nuclear stiffness were determined based on two different segments on the AFM indentation curves and were correlated with simultaneous confocal Z-stack microscopy reconstructions. On the basis of direct intracellular measurement, we show that the isolated nuclei from fibroblast-like cells exhibited significantly lower Young's moduli than intact nuclei *in situ*. We also show that there is *in situ* nucleus softening in the highly metastatic bladder cancer cell line T24 when compared to its less metastatic counterpart RT4. This technique has potential to become a reliable quantitative measurement tool for intracellular mechanics studies.

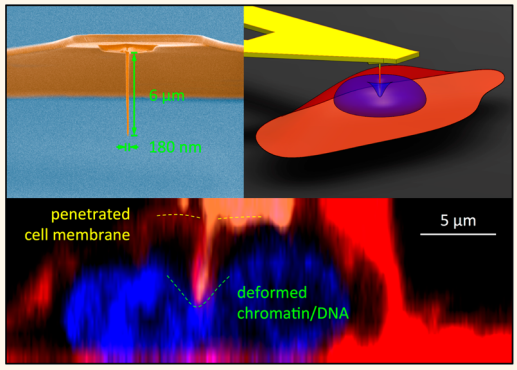

KEYWORDS: nuclear mechanics · cell stiffness · nuclear stiffness · intact nucleus · cancer cell · membrane penetration · atomic force microscopy

How does nuclear mechanics play a role in cellular mechanotransduction? A number of studies have established that nuclear mechanics significantly evolves during many normal processes such as development, differentiation and aging, and also under pathological conditions.[1−4] The nuclear lamina (also termed the *nucleoskeleton*) and heterochromatin are the major mechanical components that regulate the viscoelastic properties of nuclei.[5,6] Notably, the nuclear lamina not only acts as scaffold for the nucleus but also appears to interact closely with the genome.[7] It has been shown that the level of lamin-A (the major structural component of lamina) expression significantly influences mesenchymal stem cell lineage differentiation.[8] However, how these mechanical components play roles in global gene regulation is not well understood.

There exist mechanical connections between the extracellular matrix (ECM) and the nucleoskeleton.[9] Change in the spatial organization of chromatin (*e.g.*, due to stress) contributes prominently to its regulation.[10] Therefore, the physical environment of the cell is thought to influence intracellular and nuclear responses, including nuclear mechanics. Specifically, the nucleus has been shown to be deformed upon applied physical stimuli,[11] and the corresponding deformation and subsequent biological consequences depend in part on the mechanical properties of the nucleus.[6] Quantitative characterization of nuclear mechanical properties may provide insights for understanding mechanisms underlying cell proliferation and differentiation as well as nuclear envelope/lamina-related diseases.

Nuclei mechanical properties can be measured either with isolated nuclei or with

* Address correspondence to sun@mie.utoronto.ca, simmons@mie.utoronto.ca.

Received for review January 27, 2014 and accepted March 27, 2014.

Published online March 27, 2014
10.1021/nn500553z

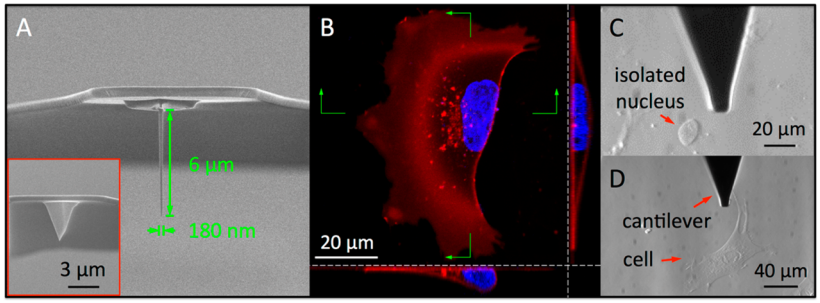

Figure 1. (A) SEM image of AFM needle tip from FIB milling of pyramidal tip (inset); (B) a fluorescent image with cross sections of cell stained for membrane (red) and nucleus (blue); optical images of AFM indentation of (C) isolated nucleus of fibroblast-like valve interstitial cell (VIC) and (D) a single intact cell (VIC).

nuclei kept in the intact cell. Measuring nuclei *in situ* is apparently advantageous in many aspects including maintenance of the cellular physiological environment because the nucleus is neither suspended nor floating within the cytosol, but instead is physically integrated with the cytoskeleton through the LINC complex.[12] However, direct measurements of nuclear mechanics *in situ* are technically challenging and were thus rarely conducted.

Several experimental techniques and tools have been utilized for studying single cell nuclear mechanics, such as micropipette aspiration (MA),[5] atomic force microscopy (AFM),[13] and substrate straining.[14] However, the fact that the nuclei were either isolated (*e.g.*, MA) or measured in an intact form but indirectly (*i.e.*, to deform the nucleus through the cell membrane and cytoplasm with, *e.g.*, MA, AFM or substrate strain) has prevented those techniques from performing direct mechanical measurements on intact cell nuclei *in situ*. The only technique that was reported for direct measurements on intact nuclei is magnetic tweezers with nanoparticles attached to the nuclear membrane;[15] however, forces exerted to the nucleus by magnetic nanoparticles are usually at the piconewton level and are often insufficient to deform the nucleus.

In this paper, we demonstrate the use of focus ion beam (FIB) to modify standard pyramidal AFM tips into sharp needle tips (Figure 1A) to penetrate the cell membrane.[16] The sharp needle tips enable direct characterization on intact cell nuclei *in situ* with minimal damage introduced to the cell. Cells were fluorescently labeled and imaged with confocal microscopy (Figure 1B) to facilitate visualizing the penetration. We then compare stiffness differences between isolated (Figure 1C) and intact (Figure 1D) nuclei. We further demonstrate that the nuclear mechanical properties of two bladder cancer cell lines correlate well with their metastatic efficiency. Cellular stiffness has been used to identify cancerous cells, based on altered Young's modulus values compared to benign cells.[17,18] Cancer progresses with the reorganization or disruption of the cytoskeleton, which results in altered cancer cell stiffness and metastatic efficiency.[19] We previously reported the cellular difference in mechanical properties of two bladder cancer cell lines, T24 and RT4.[20] T24 is a cell line derived from poorly differentiated (grade III, invasive) human bladder carcinoma,[21] and RT4 is from a grade I urothelial carcinoma (noninvasive; sometimes termed papilloma).[22] These two cell lines represent two extremes of the bladder carcinoma spectrum.

T24 and RT4 cell lines are known to exhibit different human leukocyte antigen profiles,[23] growth and migration characteristics,[24] receptor expressions and morphological features,[25,26] and *in vitro* responsiveness to chemotherapeutic agents, such as mitomycin C (MMC).[27] From the mechanics prospective, we previously found that RT4 cells exhibit significantly higher Young's moduli than T24 cells, revealing that invasive T24 has reduced stiffness compared to noninvasive RT4. Furthermore, we have also shown the difference in the F-actin content and its distribution/reorganization within these two cell lines, implying a difference in cellular internal stress.

Since the nucleus is shown to be able to sense and remodel itself to maintain tensional homeostasis when exposed to mechanical stimuli,[8,11] we hypothesized that nuclear mechanical properties would differ between the T24 and RT4 cell lines, in correlation with their different F-actin content and organization. Therefore, by applying the AFM needle tip technique, we characterized and compared the mechanical properties of *in situ* nuclei between RT4 and T24 cells. The characterization results, for the first time, quantitatively demonstrated that intact nuclei *in situ* have higher stiffness than isolated nuclei, intact nuclei are significantly stiffer than the cytoplasm, and the intact nuclei of RT4 cells have significantly higher Young's moduli than those of T24 cells.

RESULTS AND DISCUSSION

Figure 2 shows typical AFM force-displacement data including approach (blue) and retract (red) curves, indicating successful penetration of the sharp needle tip into the cell membrane and nucleus. The approach curve has four distinct segments (separated by dashed

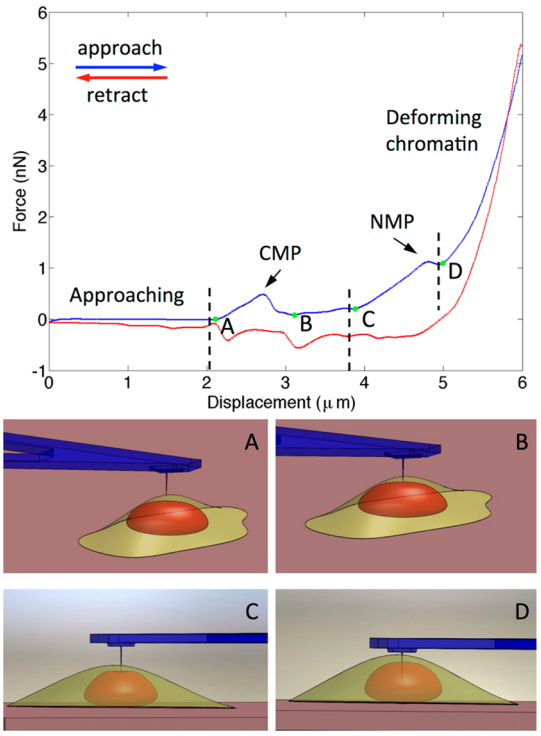

Figure 2. (Top) Experimental AFM data with two distinct force relaxations during cell membrane penetration (CMP) and nuclear membrane penetration (NMP). (Bottom) Schematic diagrams showing (A) the needle tip (blue) touching the cell membrane (yellow), (B) the needle tip having penetrated the cell membrane but before contacting the nuclear membrane (red), (C) the needle tip deforming the nucleus, and (D) the needle tip having penetrated both the cell and nuclear membranes.

lines in Figure 2), each having a characteristic slope that corresponds to four different stages in the AFM needle penetration process. The "Approaching" segment (before point A on Figure 2) is largely flat because the AFM needle tip has not made contact with the cell membrane. The "CMP" (cell membrane penetration) segment suggests that the needle tip touches the cell membrane, deforms it, and then penetrates the membrane when the AFM cantilever tip is further lowered (denoted by the slope changing point A and the peak force relaxation, Figure 2).

After the cell membrane is penetrated, the needle tip loads the nucleus and finally penetrates the nuclear envelope (denoted by the slope changing point C and the peak force relaxation, Figure 2). The second peak force relaxation was similarly used to indicate tip penetration into the nucleus as in a previous report.[28] The corresponding "NMP" (nuclear membrane penetration) segment on the force-displacement curve shows a different slope compared to the slope in segment "CMP". These two segments are used to interpret the stiffness of intact nucleus *in situ* and the stiffness of whole cell, respectively. The distance between the slope changing points in segment "CMP" and "NMP" indicates the distance between the undeformed cell membrane and nuclear membrane. The rapid upward slope at the end of the force curve (denoted by "Deforming chromatin", Figure 2) can be attributed to the eventual contact between the cantilever base and cell membrane,[16] and interactions between the needle tip and deformed chromatin (Figure 4C in blue). Once the set-point trigger force, which is the amount of force applied to the cell by the end of indentation, is reached, the needle tip is then triggered to retract from the cell.

In order to visualize cell membrane penetration and confirm the direct nuclear measurement *in situ*, our AFM was mounted onto an inverted laser scanning confocal microscope. As shown in Figures 3 and 4, the final positions of the AFM needle tip relative to the cell by the end of indentation were captured by confocal microscopy *via* Z-stack reconstruction. Figure 3 shows two typical images of reconstructed confocal cross section and the corresponding force curve indicating the needle tip deforming the cell membrane (Figure 3A) and the penetration of needle tip through the cell membrane and nuclear deformation (Figure 3B), respectively.

The large deformation of the cell membrane around the needle tip (arrows in Figure 3A) suggests that the needle tip has not penetrated the cell membrane. This can be verified by the corresponding force curve where no peak force relaxation exists. In contrast, the little deformation of the cell membrane around the needle tip (Figure 3B) suggests that the membrane relaxed and returned to the original position after needle penetration. The distance between the final position of the cell membrane and the end of the needle tip (Figure 3B) matches the penetration depth of the needle tip calculated from the force curve (cantilever deflection neglected), confirming that the membrane indeed returned to the original position. Membrane penetration was also indicated by the peak force relaxation in the corresponding force curve (Figure 3B). Notably, on the corresponding force curve in Figure 3B there was no force relaxation observed after cell membrane penetration. This implies that the needle tip has not penetrated the nuclear envelope, which is also suggested by the deformation of the chromatin (dashed line in Figure 3B) and the indentation of the laterally tensioned nuclear envelope.

Figure 4 shows a typical image of the needle tip penetration through both the cell membrane and the nuclear envelope and the corresponding force curve of the process. Similarly, the cell membrane penetration was indicated by both the little deformation of the membrane around the needle tip (white arrows) and the first peak force relaxation (green arrow, Figure 4A). It was consistently observed that the contour of the Hoechst stained chromatin only deformed locally around the needle tip (green arrows Figure 4C). In contrast to the more global deformation shown in

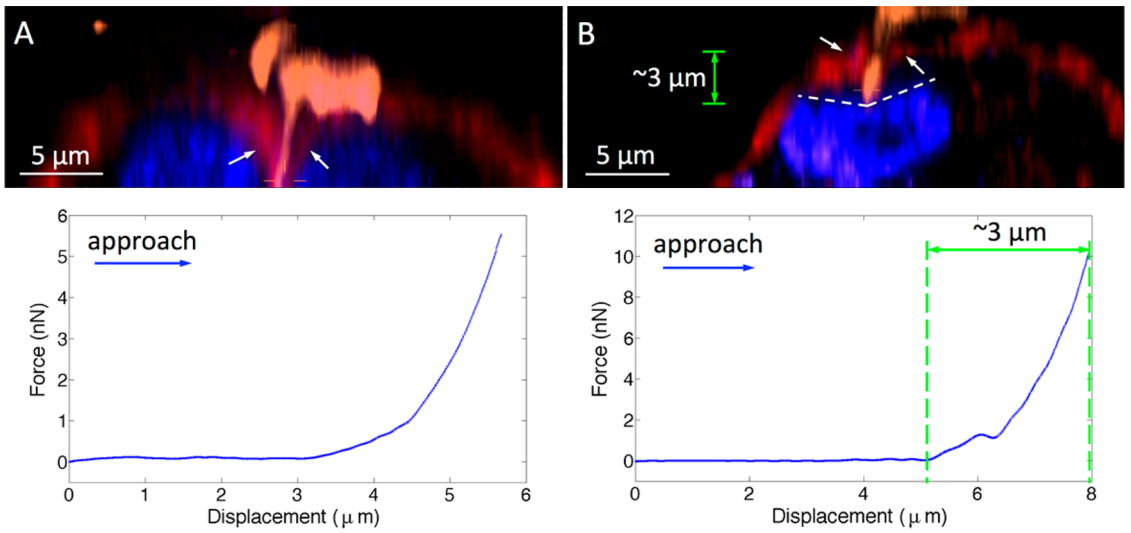

Figure 3. Reconstructed Z-stack confocal images showing the final location of the AFM needle tip relative to the cell by the end of indentation when the trigger force was reached, and corresponding experimental force curves. (A) Cell membrane deformation (membrane in red) suggested by the large deformation of cell membrane around the needle tip (tip in orange) (white arrows) and also by absent force relaxation in the force-displacement curve below; (B) cell membrane penetration suggested by the little deformation of cell membrane around the needle tip (white arrows) and also by the presence of a significant force relaxation in the force curve; this is confirmed by the match between the distance from the final position of the cell membrane to the end of the needle tip (confocal image; ~3 μm) and the penetration depth of the needle tip (force curve; ~3 μm). The nuclear deformation (nucleus in blue) denoted with white dashed line and also confirmed by the absence of force relaxation after cell membrane penetration.

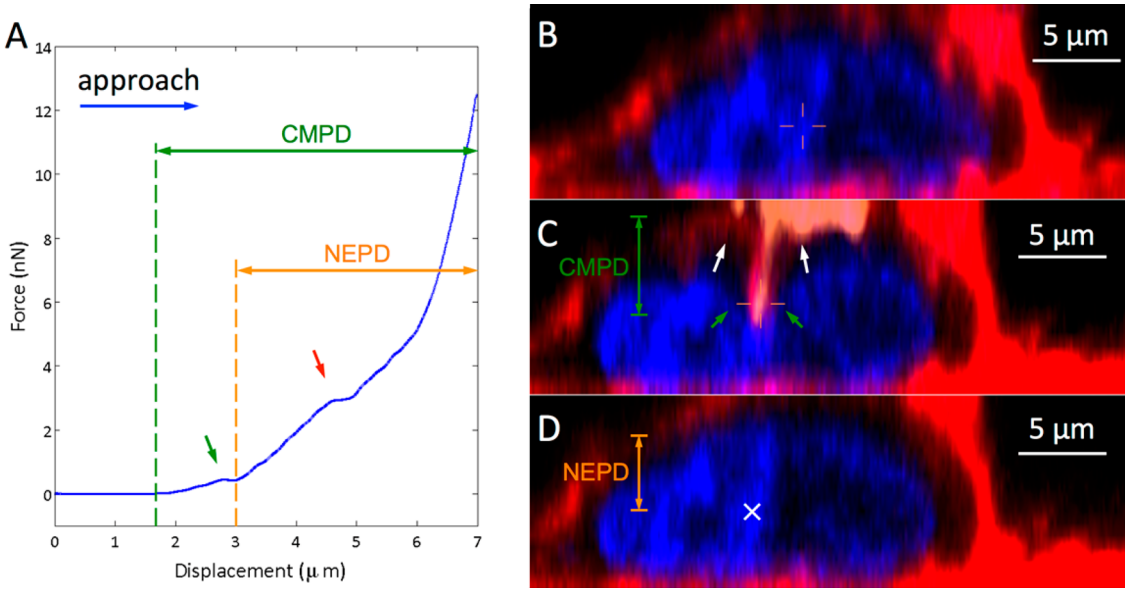

Figure 4. Experimental force curve (A) showing double peak force relaxation indicating penetration of both cell and nuclear membranes. CMPD, cell membrane penetration distance; NEPD, nuclear envelope penetration distance. (B–D) Z-stack confocal images of the same cell corresponding to the force curve showing (B) before the needle tip indentation, (C) the final location of needle tip relative to the cell by the end of indentation when the trigger force set-point was just reached, and (D) after the needle tip has been retracted from the cell. The × symbol in (D) marks the final position of the end of the needle tip.

Figure 3B, the local deformation of the chromatin is likely caused by the local force applied directly by the needle tip, implying nuclear envelope penetration. Furthermore, the corresponding force curve (Figure 4A) shows a second peak force relaxation (red arrow) that also indicates nuclear envelope penetration because the solid-like structure of continuous nuclear envelope and meshed nuclear laminar would allow the stress to accumulate until the compressibility limit is exceeded and the structure collapses.[29,30] Interestingly, instead of insertion into the nuclear chromatin, the needle tip only caused deformation of the chromatin implying the highly integrated structure of the condensed chromatin. Another explanation of this could be that

the nucleoplasm surrounding chromatin preventing the needle from inserting into the chromatin since it has been shown to be highly viscous.[31]

Therefore, a successful penetration through cell membrane can be confirmed by both the first peak force relaxation on the force-displacement curve and the undeformed cell membrane shape around the tip from confocal imaging. However, without the nuclear envelope specifically labeled, nuclear envelope penetration currently can only be inferred based on the second peak force relaxation on the force curve and can be additionally supported by the chromatin local deformation from confocal imaging. On the basis of the above criteria of force relaxation, the successful penetration rates of cell membrane alone and both cell and nuclear membrane were 90% and 34% for 30 VICs tested, 77.8% and 35.6% for 28 T24 cells tested, and 66% and 37.1% for 27 RT4 cells tested, respectively. To achieve needle tip penetration, it was found that tip velocity higher than 10 μm/s and trigger force larger than 5 nN were needed. Tip change/cleaning proved useful for minimizing the effect of tip contamination, and aligning the tip with the center of the nucleus also helped distinguish the two peak force relaxations on the force curve.

Furthermore, the slope changing points on the force-displacement curves correlated well with the cross-sectional shapes of the cells in the confocal images (Figures 3 and 4). This supports the hypothesis that the slope change in the AFM indentation force curve is due to the change from initial tip contact with the cell membrane to contact with the nuclear envelope. The penetration depths, which are the distances of the slope changing points to the end of the curve subtracted by cantilever deflection (which ranged from 160 to 400 nm), matched the distances between the undeformed position of the cell membrane or the nuclear envelope and the final position of the tip of the needle in the confocal images (termed cell membrane penetration distance (CMPD) and nuclear envelope penetration distance (NEPD), respectively, Figure 4). This confirms that the segments led by each slope changing point indeed correspond to the indentation of each of the two phospholipid bilayers and therefore can be used to calculate the Young's moduli of the cell and the nucleus, respectively. It is expected that the Young's moduli measured with these needle tips will be higher than those measured with spherical tips in a previous report.[20] This discrepancy is attributable to the fact that AFM needle tips generate large local strains which would result in hyper-elastic strain stiffening of the cells.[32,33]

The confocal images were also used to evaluate the impact of needle tip penetration on cell integrity. Figure 4B,D shows the same cross section of the same cell where the AFM needle tip was being inserted, before and after penetration. There was no observable disruption on either the cell membrane or the nucleus. In addition, cell viability following nuclear measurements was confirmed through trypan blue vital staining. All the tested cells were clear of trypan blue staining, indicating high cell viability, which is in agreement with other studies using similar or slightly larger-sized nanoinjectors than our AFM needle tip.[34,35] Compared to other experimental techniques that are used to study nuclear mechanics, AFM needle tip penetration provides a better solution for characterizing the nucleus *in situ* without causing unrecoverable damage to the primary cell structures.

To test whether the physical connection with the cytoskeleton has an impact on nuclear mechanical properties, we employed the AFM needle tips to perform measurements on isolated VIC nuclei and nuclei within intact VICs. The isolated VIC nuclei exhibited much lower stiffness compared to the intact nuclei (9.29 ± 1.80 *vs* 26.54 ± 3.41 kPa on soft substrate, $p < 0.05$; *vs* 84.36 ± 16.16 kPa on stiff substrate, $p < 0.05$, Figure 5A). It was proposed that the nucleus bears intracellular stresses and has pre-existing strain *in situ*.[36] Hence, it is imaginable that nucleus would undergo a morphological and/or stiffness change when the surrounding mechanical environment is altered. Deguchi *et al.* demonstrated a significant reduction in

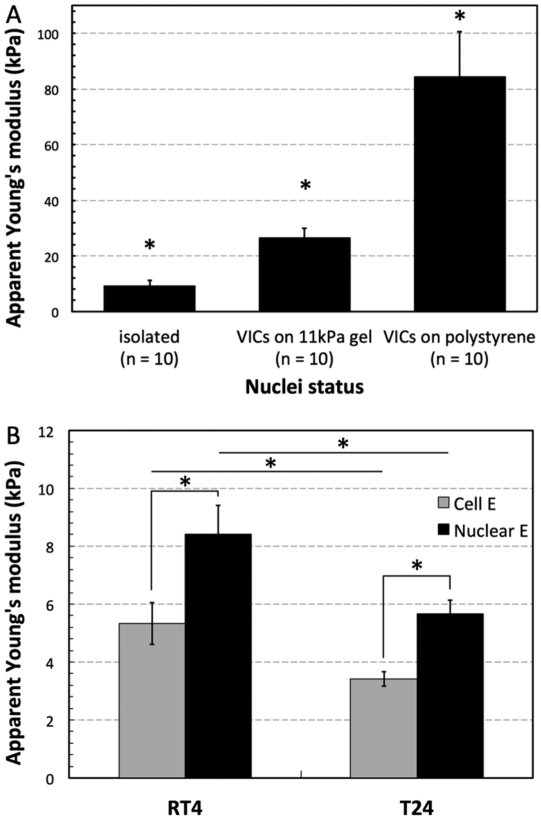

Figure 5. Experimental data comparing modulus values of (A) isolated nuclei ($n = 10$) and intact nuclei on soft ($n = 10$) and stiff ($n = 10$) substrates *in situ* (*$p < 0.05$ for all pairwise comparisons); and (B) RT4 ($n = 10$) and T24 ($n = 10$) cells and their intact nuclei (*$p < 0.03$).

cross-sectional area of the endothelial cell nuclei immediately after isolation and thus proposed that the endothelial cell nuclei were vertically compressed in cytoplasm under static conditions.[37] Therefore, our measured stiffness reduction of the isolated VIC nuclei could be attributable to the release from a prestressed state to a zero-stress state.

Mechanical connections between the nucleus and the cytoskeleton distort the nuclear envelope under prestress and may even evoke transcriptional changes by locally altering the spatial accessibility of chromatin to transcriptional regulators.[10] Such changes are expected to be positively correlated to the extent of the distortion.[38] By measuring nuclear stiffness in intact VICs cultured on soft (*i.e.*, 11 kPa) and rigid (*i.e.*, polystyrene) substrates, our experiments showed that the substrate stiffness also influenced nuclear stiffness (Figure 5A, $*p < 0.05$). We previously showed that the stiffness of the substrates on which VICs are seeded correlated positively with the formation of actin stress fibres,[32] implying increased nuclear stiffness measured here with increased cytoskeletal tension. Additionally, nuclear stiffening on stiff substrates may reflect alterations in the amount and conformation of lamin-A.[8] Although it is understood that due to the finite cell thickness, substrate deformability could post additional error to the estimated Young's modulus in AFM indentation measurements, it has been shown that the error is reasonably small so that it will not mask the trends of relative comparisons here.[32]

Finally, we examined the nuclear mechanical properties of two bladder cancer cell lines in light of previous observations of their reorganization of F-actin.[20] The AFM needle tips were used to measure the Young's moduli of the intact nuclei of RT4 ($n = 10$) and T24 ($n = 10$) cells. The results showed that the nuclei of both cell lines exhibited significantly ($p < 0.0004$) higher stiffness than the cell membrane/cytoplasm (8.4 ± 1.02 *vs* 5.33 ± 0.73 kPa for RT4; 5.67 ± 0.48 *vs* 3.42 ± 0.26 kPa for T24, Figure 5B). Moreover, the average Young's modulus of intact nuclei of RT4 cells was higher than that of nuclei from T24 (8.4 ± 1.02 *vs* 5.67 ± 0.48 kPa, $p < 0.03$, Figure 5B). These data show that the less metastatic RT4 cells not only exhibit higher whole cell stiffness, but also have stiffer nuclei compared to T24 cells that have a higher grade metastatic potential. The positive correlation between cell and nuclear stiffness measured *in situ* for RT4 and T24 is thus revealed for the first time, although it is not understood whether the softening of T24 nuclei depends on the softening of T24 cytoplasm or not.

Swift *et al.* showed that the abundance of nuclear protein lamin-A in the mesenchymal nuclear lamina is a major determinant of nuclear physical properties and cell differentiation.[8] It has also been observed that increased cytoskeletal tension reduces the turnover of lamin-A in the nuclear lamina and the increased lamin-A in turn stiffens the nucleus and enhances osteogenesis.[8] This suggests that the increase in lamin-A, manifested as nuclear physical stiffening, can be an important part of cellular response to the increased tension from the ECM. In addition, micropipette aspiration of cell nuclei has shown that lamin-A indeed confers nuclear stiffness and impedes nuclear deformation under mechanical stress.[8] Therefore, the difference in average nuclear stiffness between RT4 and T24 cells is likely caused at least partially by the difference in lamina composition, including lamin-A. However, in the process of progressing into highly cancerous cells like T24, whether the bladder cancer cell nuclei function in a similar mechanism as mesenchymal nuclei in response to reduced tension needs further study.

This technique can also be potentially used to characterize the nuclear mechanical properties of cells in three-dimensional (3D) matrix to gain better understanding of mechanobiology of cell nuclei in a more physiologically relevant microenvironment. However, this would require increased length of AFM needle tip to reach the embedded cells and appropriate interpretation of force–indentation data since interactions between the needle tip and the 3D matrix would be even more complex.

CONCLUSIONS

We demonstrate that AFM needle penetration can be used to perform intracellular characterization of cell nuclei *in situ*. Force-displacement data are obtained when the needle tip deforms the cell membrane and nuclear envelope. The results quantitatively show differences in the stiffness of isolated nuclei *vs* intact nuclei, nuclei *vs* cytoplasm, nuclei of cells cultured on substrates of different stiffness, and nuclei of cancer cells having different metastatic potential. The main advantage of this technique for studying nuclear mechanics is the preservation of the integrity of the cell structure and the LINC complex. This technique can be utilized to gain insight into the mechanisms by which cell nuclei respond to biochemical and biophysical stimuli as well as physiological and pathological changes, and how nuclear mechanics influences cell function and development.

METHOD AND MATERIALS

Cell Culture. For comparison between intact and isolated nuclei, fibroblast-like valve interstitial cells (VICs) were selected as our cell model since they have abundant cytoskeleton filaments. VICs were seeded at 10 000 cells/cm^2 and cultured on tissue culture-treated polystyrene with complete medium

(Dulbecco's modified Eagle's medium (DMEM) with 10% fetal bovine serum (FBS) and 1% penicillin−streptomycin). Cells were incubated at 37 °C and 5% CO_2, and subcultured when close to confluency up to passage three. Before AFM and confocal experiments, VICs were passaged and seeded to 35 mm Petri dishes and 50 mm glass bottom dishes (P50G-0-30-F, MatTek corp, MA; and GWSt-5040, WillCo Wells BV, The Netherlands), respectively, at 2500 cells/cm^2 and cultured for 24 h so that single cells could be located. In some experiments, polyacrylamide (PA) gel was used as the soft culture substrate. VICs were grown on PA hydrogels with compressive elastic (Young's) moduli of 11 kPa and coated with type I collagen, as described previously.[39] Cellular and nuclear stiffness were measured on VICs cultured on both Petri dishes and PA gel substrates.

T24 and RT4 cells were obtained from the American Type Culture Collection (ATCC, Manassas, VA). Cells were cultured in ATCC-formulated McCoy's 5a modified medium with 10% FBS and 1% penicillin−streptomycin at 37 °C and 5% CO_2. Subculture was conducted before cells reached confluency. Similarly to VICs, before AFM and confocal experiments, T24 and RT4 cells were passaged and seeded at 2500 cells/cm^2 in 35 mm Petri dishes and 50 mm glass bottom dishes, respectively, for 24 h.

VIC Nuclei Isolation. VICs of passage 2−3 were removed from the Petri dishes by gently scraping with a cell lifter and transferred to a prechilled conical tube after they were rinsed with nuclear extraction buffer (Active Motif). The cell suspension was subsequently centrifuged for 5 min at 500 rpm, and the resulting pellet was resuspended in 1× hypotonic buffer (40010 and 40410, Nuclear Extract Kit, Active Motif) and incubated on ice for 15 min. Detergent (40010 and 40410, Nuclear Extract Kit, Active Motif) was added directly into the incubated cell suspension, and then the nuclei were separated from the cellular debris after 30 s centrifugation at 14 000*g* at 4 °C. The supernatant (cytoplasmic fraction) was discarded and the pellet (containing nuclei) was then resuspended and transferred to a 35 mm Petri dish in complete VIC culture medium for 8 h before the AFM measurements, allowing the nuclei to precipitate and weakly attach to the dish surface.

Fabrication of AFM Sharp Needle Tips. AFM sharp needle tips were formed by processing standard AFM cantilevers with a focus ion beam (FIB)-scanning electron microscope (SEM) dual beam system (FEI StrataTM DB-235). Individual AFM silicon pyramidal tips (MLCT-D, Bruker; nominal cantilever spring constant k = 0.03 N/m) were reshaped and sharpened by FIB etching and then characterized using SEM imaging. The high-aspect ratio of the sharp needle tips enables the piercing through the cell membrane and the indentation of the nuclear membrane without being disturbed by the premature contact of AFM tip base and the cell membrane surface, as observed in indentation experiments with regular pyramidal AFM tips.[40]

The pyramidal tip was cut into a thin plate by focusing the FIB on the two areas on each side of the plate. The resulting thin triangular plate was then rotated for 90° about the central axis of the original pyramid and etched in the same manner, leaving a thin needle as desired.[40] The FIB process typically takes approximately 40 min/tip. The tips are 150−250 nm in diameter and 3−6 μm in length (Figure 1A).

Cell and AFM Tip Fluorescence Staining and Confocal Laser Scanning Microscopy. *CellMask and Hoechst.* The plasma membrane of a cell was stained with the CellMask Deep Red stain (C10046, Invitrogen), and the cell nucleus was stained with the standard Hoechst dye (33258). Briefly, a fresh working solution with concentration of 10 μg/mL of CellMask and 50 μg/mL of Hoechst was prepared by mixing the two stocking solutions in warm PBS+/+ before confocal imaging. The cells were rinsed with PBS+/+ and then incubated with the stain working solution at 37 °C for 20 min. Then, the staining solution was removed, and the stained cells were further rinsed with PBS+/+ twice, after which the cells were immediately imaged with confocal microscopy (Figure 1B).

Alexa555. The AFM needle tips were first treated with plasma activation for 2 min. (3-Aminopropyl)triethoxysilane (APTES; 99%) (Sigma-Aldrich) was diluted to 2% in a mixture of 95% ethanol and 5% DI water. The tips were placed into the APTES solution for 10 min and then rinsed with ethanol, dried with N_2, and incubated at 120 °C for 1 h. The Alexa Fluor 555 NHS ester (Invitrogen) was dissolved in DMSO to 100 μg/mL and used immediately. The silanized tips were then placed into the stain solution and incubated for 1 h at room temperature, and then washed with PBS and DI water and dried with N_2.

Confocal Microscopy Imaging. Z-stack images of stained cells were acquired with a laser scanning confocal microscope (Nikon A1) using 60× oil-immersion objective (Apo 60× /1.40 Oil λS DIC N2, Nikon). The AFM was mounted on the confocal microscope. AFM was combined with confocal imaging for imaging cell/nuclear membrane deformation and penetration by the sharp AFM needle tip.

AFM Measurement and Data Analysis. Force measurements for isolated VIC nuclei, VICs, T24 and RT4 cells were all made in their culture medium at room temperature (Figure 1C,D). Measurements in each Petri dish were completed within 20 min, and cell viability was subsequently confirmed through trypan blue vital staining. Measurements were made *via* "point and shoot" and microscope image registration and overlay (MIRO) and AFM indentation (Bioscope Catalyst, Bruker), over the center of single isolated nuclei or single intact cell, so as to avoid influence from neighbor cells.

Force curves captured at the cell center (*i.e.*, over the nucleus) with distinct force relaxations (corresponding to cell membrane and nuclear penetration) were used to estimate the Young's modulus of the cell and the nucleus. While a single peak in the force−indentation curve indicated the penetration of the nuclear envelope for the isolated VIC nuclei, two force relaxations were observed in whole cell force measurements resulting from the penetration of both the cell and nuclear membrane.

The Hertz model for a cylindrical tip (assuming the fabricated needle tips approximate a cylindrical shape) was applied to fit the rising slopes of the approach curve before relaxation.[32] The relationship between the indentation depth, h, and the loading force, F is $F = 2a[E/(1 - v^2)]h$, where E is the Young's modulus of the sample, v is the Poisson ratio of the sample, and a is the radius of the indenting cylinder. The apparent Young's moduli for isolated VIC nuclei, cell cytoplasm and intact nuclei are reported as mean ± standard error of the mean and were analyzed by one-way ANOVA and Student−Newman−Keuls test for pairwise comparisons in SigmaPlot 11.0. The statistical significance in each comparison was evaluated with $p \leq 0.05$ to denote significance.

Conflict of Interest: The authors declare no competing financial interest.

Acknowledgment. The authors acknowledge financial support from the NSERC CREATE Program in Microfluidic Applications and Training in Cardiovascular Health (MATCH) (H.L.), the Natural Science and Engineering Research Council of Canada and the Canada Research Chairs program in Mechanobiology (C.A.S.) and Micro- and Nano-Engineering Systems (Y.S.).

REFERENCES AND NOTES

1. Worman, H. J.; Courvalin, J.-C. Nuclear Envelope, Nuclear Lamina, and Inherited Disease. *Int. Rev. Cytol.* **2005**, *246*, 231–279.
2. Zwerger, M.; Ho, C. Y.; Lammerding, J. Nuclear Mechanics in Disease. *Annu. Rev. Biomed. Eng.* **2011**, *13*, 397–428.
3. Hampoelz, B.; Lecuit, T. Nuclear Mechanics in Differentiation and Development. *Curr. Opin. Cell Biol.* **2011**, *23*, 668–675.
4. Rowat, A. C.; Lammerding, J.; Ipsen, J. H. Mechanical Properties of the Cell Nucleus and the Effect of Emerin Deficiency. *Biophys. J.* **2006**, *91*, 4649–4664.
5. Guilak, F.; Tedrow, J. R.; Burgkart, R. Viscoelastic Properties of the Cell Nucleus. *Biochem. Biophys. Res. Commun.* **2000**, *269*, 781–786.
6. Martins, R. P.; Finan, J. D.; Guilak, F.; Lee, D. A. Mechanical Regulation of Nuclear Structure and Function. *Annu. Rev. Biomed. Eng.* **2012**, *14*, 431–455.
7. Martins, R. P.; Krawetz, S. A. Decondensing the Protamine Domain for Transcription. *Proc. Natl. Acad. Sci. U. S. A.* **2007**, *104*, 8340–8345.

8. Swift, J.; Ivanovska, I. L.; Buxboim, A.; Harada, T.; Dingal, P. C. D. P.; Pinter, J.; Pajerowski, J. D.; Spinler, K. R.; Shin, J.-W.; Tewari, M.; *et al.* Nuclear Lamin-A Scales with Tissue Stiffness and Enhances Matrix-Directed Differentiation. *Science* **2013**, *341*, 1–15.
9. Maniotis, A. J.; Chen, C. S.; Ingber, D. E. Demonstration of Mechanical Connections between Integrins, Cytoskeletal Filaments, and Nucleoplasm That Stabilize Nuclear Structure. *Proc. Natl. Acad. Sci. U. S. A.* **1997**, *94*, 849–854.
10. Mazumder, A.; Shivashankar, G. V. Emergence of a Prestressed Eukaryotic Nucleus during Cellular Differentiation and Development. *J. R. Soc., Interface* **2010**, *7* (Suppl. 3), S321–D330.
11. Wang, N.; Tytell, J. D.; Ingber, D. E. Mechanotransduction at a Distance: Mechanically Coupling the Extracellular Matrix with the Nucleus. *Nat. Rev. Mol. Cell Biol.* **2009**, *10*, 75–82.
12. Crisp, M.; Liu, Q.; Roux, K.; Rattner, J. B.; Shanahan, C.; Burke, B.; Stahl, P. D.; Hodzic, D. Coupling of the Nucleus and Cytoplasm: Role of the LINC Complex. *J. Cell Biol.* **2006**, *172*, 41–53.
13. Azeloglu, E. U.; Bhattacharya, J.; Costa, K. D. Atomic Force Microscope Elastography Reveals Phenotypic Differences in Alveolar Cell Stiffness. *J. Appl. Physiol.* **2008**, *105*, 652–661.
14. Lammerding, J.; Hsiao, J.; Schulze, P. C.; Kozlov, S.; Stewart, C. L.; Lee, R. T. Abnormal Nuclear Shape and Impaired Mechanotransduction in Emerin-Deficient Cells. *J. Cell Biol.* **2005**, *170*, 781–791.
15. Bausch, A. R.; Möller, W.; Sackmann, E. Measurement of Local Viscoelasticity and Forces in Living Cells by Magnetic Tweezers. *Biophys. J.* **1999**, *76*, 573–579.
16. Obataya, I.; Nakamura, C.; Han, S.; Nakamura, N.; Miyake, J. Nanoscale Operation of a Living Cell Using an Atomic Force Microscope with a Nanoneedle. *Nano Lett.* **2005**, *5*, 27–30.
17. Suresh, S.; Spatz, J.; Mills, J. P.; Micoulet, A.; Dao, M.; Lim, C. T.; Beil, M.; Seufferlein, T. Connections between Single-Cell Biomechanics and Human Disease States: Gastrointestinal Cancer and Malaria. *Acta Biomater.* **2005**, *1*, 15–30.
18. Guck, J.; Schinkinger, S.; Lincoln, B.; Wottawah, F.; Ebert, S.; Romeyke, M.; Lenz, D.; Erickson, H. M.; Ananthakrishnan, R.; Mitchell, D.; *et al.* Optical Deformability as an Inherent Cell Marker for Testing Malignant Transformation and Metastatic Competence. *Biophys. J.* **2005**, *88*, 3689–3698.
19. Yamaguchi, H.; Condeelis, J. Regulation of the Actin Cytoskeleton in Cancer Cell Migration and Invasion. *Biochim. Biophys. Acta* **2007**, *1773*, 642–652.
20. Liu, H.; Tan, Q.; Geddie, W. R.; Jewett, M. A. S.; Phillips, N.; Ke, D.; Simmons, C. A.; Sun, Y. Biophysical Characterization of Bladder Cancer Cells with Different Metastatic Potential. *Cell Biochem. Biophys.* **2014**, *68*, 241–246.
21. Bubeník, J.; Baresová, M.; Viklický, V.; Jakoubková, J.; Sainerová, H.; Donner, J. Established Cell Line of Urinary Bladder Carcinoma (T24) Containing Tumour-Specific Antigen. *Int. J. cancer* **1973**, *11*, 765–773.
22. Franks, L.; Rigby, C. HeLa Cells and RT4 Cells. *Science* **1975**, *188*, 168.
23. O'Toole, C. M.; Tiptaft, R. C.; Stevens, A. HLA Antigen Expression on Urothelial Cells: Detection by Antibody-Dependent Cell-Mediated Cytotoxicity. *Int. J. cancer* **1982**, *29*, 391–395.
24. Kim, J.; Ji, M.; DiDonato, J. A.; Rackley, R. R.; Kuang, M.; Sadhukhan, P. C.; Mauney, J. R.; Keay, S. K.; Freeman, M. R.; Liou, L. S.; *et al.* An hTERT-Immortalized Human Urothelial Cell Line That Responds to Anti-Proliferative Factor. *In Vitro Cell. Dev. Biol.: Anim.* **2011**, *47*, 2–9.
25. DeGraff, D. J.; Clark, P. E.; Cates, J. M.; Yamashita, H.; Robinson, V. L.; Yu, X.; Smolkin, M. E.; Chang, S. S.; Cookson, M. S.; Herrick, M. K.; *et al.* Loss of the Urothelial Differentiation Marker FOXA1 Is Associated with High Grade, Late Stage Bladder Cancer and Increased Tumor Proliferation. *PLoS One* **2012**, *7*, No. e36669.
26. Yamada, T.; Ueda, T.; Shibata, Y.; Ikegami, Y.; Saito, M.; Ishida, Y.; Ugawa, S.; Kohri, K.; Shimada, S. TRPV2 Activation Induces Apoptotic Cell Death in Human T24 Bladder Cancer Cells: A Potential Therapeutic Target for Bladder Cancer. *Urology* **2010**, *76*, 509.e1–7.
27. Van der Heijden, A. G.; Jansen, C. F. J.; Verhaegh, G.; O'donnell, M. A.; Schalken, J. A.; Witjes, J. A. The Effect of Hyperthermia on Mitomycin-C Induced Cytotoxicity in Four Human Bladder Cancer Cell Lines. *Eur. Urol.* **2004**, *46*, 670–674.
28. Han, S.-W.; Nakamura, C.; Kotobuki, N.; Obataya, I.; Ohgushi, H.; Nagamune, T.; Miyake, J. High-Efficiency DNA Injection into a Single Human Mesenchymal Stem Cell Using a Nanoneedle and Atomic Force Microscopy. *Nanomedicine* **2008**, *4*, 215–225.
29. Rowat, A. C.; Foster, L. J.; Nielsen, M. M.; Weiss, M.; Ipsen, J. H. Characterization of the Elastic Properties of the Nuclear Envelope. *J. R. Soc., Interface* **2005**, *2*, 63–69.
30. Dahl, K. N.; Kahn, S. M.; Wilson, K. L.; Discher, D. E. The Nuclear Envelope Lamina Network Has Elasticity and a Compressibility Limit Suggestive of a Molecular Shock Absorber. *J. Cell Sci.* **2004**, *117*, 4779–4786.
31. Khanna, P. *Cell and Molecular Biology*; I.K. International Publishing House Pvt. Limited: New Delhi, India, 2008; p. 219.
32. Liu, H.; Sun, Y.; Simmons, C. A. Determination of Local and Global Elastic Moduli of Valve Interstitial Cells Cultured on Soft Substrates. *J. Biomech.* **2013**, *46*, 1967–1971.
33. Dokukin, M. E.; Sokolov, I. On the Measurements of Rigidity Modulus of Soft Materials in Nanoindentation Experiments at Small Depth. *Macromolecules* **2012**, *45*, 4277–4288.
34. Yoo, S. M.; Kang, M.; Kang, T.; Kim, D. M.; Lee, S. Y.; Kim, B. Electrotriggered, Spatioselective, Quantitative Gene Delivery into a Single Cell Nucleus by Au Nanowire Nanoinjector. *Nano Lett.* **2013**, *13*, 2431–2435.
35. Wang, W.; Sun, Y.; Zhang, M.; Anderson, R.; Langille, L.; Chan, W. A System for High-Speed Microinjection of Adherent Cells. *Rev. Sci. Instrum.* **2008**, *79*, 104302.
36. Ingber, D. E. Tensegrity: The Architectural Basis of Cellular Mechanotransduction. *Annu. Rev. Physiol.* **1997**, *59*, 575–599.
37. Deguchi, S.; Maeda, K.; Ohashi, T.; Sato, M. Flow-Induced Hardening of Endothelial Nucleus as an Intracellular Stress-Bearing Organelle. *J. Biomech.* **2005**, *38*, 1751–1759.
38. Wang, J. H.-C.; Thampatty, B. P.; Lin, J.-S.; Im, H.-J. Mechanoregulation of Gene Expression in Fibroblasts. *Gene* **2007**, *391*, 1–15.
39. Chen, J.-H.; Chen, W. L. K.; Sider, K. L.; Yip, C. Y. Y.; Simmons, C. A. B-Catenin Mediates Mechanically Regulated, Transforming Growth Factor-B1-Induced Myofibroblast Differentiation of Aortic Valve Interstitial Cells. *Arterioscler., Thromb., Vasc. Biol.* **2011**, *31*, 590–597.
40. Obataya, I.; Nakamura, C.; Han, S.; Nakamura, N.; Miyake, J. Mechanical Sensing of the Penetration of Various Nanoneedles into a Living Cell Using Atomic Force Microscopy. *Biosens. Bioelectron.* **2005**, *20*, 1652–1655.